Applied Surface Science xxx (2018) xxx–xxx

Contents lists available at ScienceDirect

Applied Surface Science

journal homepage: www.elsevier.com/locate/apsusc

Full Length Article

Hierarchically porous carbon derived from biomass: Effect of mesopore and heteroatom-doping on electrochemical performance

Hongying Quan[a], Xiaoyu Fan[b,*], Wenxiu Wang[a,c], Weimin Gao[c], Yinghu Dong[a], Dezhi Chen[c,*]

[a] School of Materials Science and Engineering, Nanchang Hangkong University, Nanchang 330063, China
[b] NanoSolutions Co.Ltd. Beijing, 100027, China
[c] Key Laboratory of Jiangxi Province for Persistent Pollutants Control and Resources Recycle, School of Environmental and Chemical Engineering, Nanchang Hangkong University, Nanchang 330063, China

ARTICLE INFO

Article history:
Received 18 October 2017
Received in revised form 14 January 2018
Accepted 23 January 2018
Available online xxx

Keywords:
Biomass
Hierarchical pore
Heteroatomic doping
Electrode materials
Supercapacitors

ABSTRACT

Two kinds of porous carbons derived from *Osmanthus fragrans* and *Sterculia lychnophora,* respectively, are prepared by hydrothermal carbonization and KOH activation. The characterizations of electron microscopy and N_2 adsorption-desorption isotherms show that both *Osmanthus fragrans*-derived porous carbon and *Sterculia lychnophora*-derived porous carbon have the hierarchical micro/meso/macroporous structure with interpenetrating network, but pore structure is mainly the micropore for *Osmanthus fragrans*-derived porous carbon, while more mesopore for *Sterculia lychnophora*-derived porous carbon. The surface chemical analysis reveals that *Sterculia lychnophora*-derived porous carbon has C—N and more oxygen-containing groups in comparison with the *Osmanthus fragrans*-derived porous carbon. When used as electrode materials for EDLC, the *Sterculia lychnophora*-derived porous carbon electrodes deliver higher specific capacitance, higher capacitance retention and better cycling stability than *Osmanthus fragrans*-derived porous carbon. The superior electrochemical performance of *Sterculia lychnophora*-derived porous carbon is mainly attributed to the abundant mesopore, doping of N atom as well as more oxygen-containing groups. Finally, symmetrical supercapacitors are assembled by *Sterculia lychnophora*-derived porous carbon electrodes and release a high energy density of 9.58 W h kg^{-1} with a powder density of 500 W kg^{-1}. The results showed that preparation of porous carbon materials from biomass is effectively procedure to improve high performance ELDC devices, and the selection of biomass precursors is the key in the preparation high performance electrode materials for ELDC.

1. Introduction

Electrical double layer capacitors (EDLC), where the energy storage arises from the accumulation of electrostatic charge at the interfaces between electrode and electrolyte, have arouse great concern since they can deliver high powder density, very fast charging/discharging kinetics, unlimited long cycle life and bipolar operational flexibility [1–3]. In generally, porous activated carbons [2,4], carbon nanofibers [5,6], carbon nanotubes [7], carbon nanobelts [8] and graphene [9,10] have been intensively investigated for EDLC applications. Among these carbon materials, porous activated carbon is an ideal material for EDLCs due to its large surface area and good electrical conductivity [2,11–15]. At present, traditional porous activated carbons (AC) have been successfully developed as electrodes for commercial EDLC devices. However, the much low energy densities (approximately 5 Wh kg^{-1}) of commercial EDLC devices have hindered their wide applications. It is mainly attributed to that the pore structure in traditional activated carbon materials with high specific surface area more than 3000 m^2 g^{-1} are predominantly microporous (pore width <2 nm), which limits the rapid ion diffusion and transport especially at high current density [12,16].

To develop a high-performance porous carbon EDLC devices, introducing macropores (>50 nm) and mesopores (pore width of 2–50 nm) into porous carbon can improve the utilization of the pore surface area and accelerate mass transfer to enhance the power density and energy density [12,14,17]. Recently, the doping of heteroatom such as O and N to carbon materials has drawn broad interesting because that the heteroatoms can change the electron donor-acceptor features of carbon materials, and accordingly enhance the wettability of carbon materials and improve the elec-

* Corresponding authors.
E-mail addresses: fanxy@bjhed.net (X. Fan), chendz@nchu.edu.cn, chendz@buaa.edu.cn (D. Chen).

https://doi.org/10.1016/j.apsusc.2018.01.202
0169-4332/

tric conductivity and capacitance behaviors [1,18–22]. Therefore, the design of hierarchically micro/meso/macroporous carbon with doping of electron-donating element has emerged as a promising field of further investigation with an extensive scope. However, it is still an arduous work and mostly expectant to design and fabricate carbon materials with suitable hierarchical pore and the doping of heteroatom in a governable and practicable way, which can improve the electrochemical performance of EDLC owing to its capability to tailor the physical/chemical properties of the electroactive materials.

Recently, biomass has been extensively used as precursor to prepare the heteroatom doped carbon materials with special hierarchical pore structure [15,23–30]. However, the reported results showed that the porous carbons derived from different biomass delivered very different electrochemical performance as electrode materials for EDLC because of different microstructure and heteroatom doping. Therefore, the selection of biomass precursor is very important in the preparation of high-performance electrode materials for EDLC. Moreover, the effect of pore structure and the doping of heteroatom on the electrochemical performance is still needing to clarify. Herein, hierarchically porous carbons were prepared using two kinds of biomasses (*Osmanthus fragrans* and *Sterculia lychnophora*) as precursors by a simple two-step method including hydrothermal carbonization and KOH activation, and the effect of heteroatom-doping and mesopore on the electrochemical behavior of the as-prepared porous carbons was clarified in detail.

2. Experimental section

2.1. Preparation of porous carbon

Osmanthus fragrans-derived porous carbon (OPC) and *Sterculia lychnophora* derived porous carbon (SPC) were prepared through two-step strategy of hydrothermal carbonization and KOH activation. First, dry *Osmanthus fragrans* (0.5 g) and *Sterculia lychnophora* powder (0.5 g) was added with 30 mL distilled water, respectively, and then placed in a 50 mL Teflon lined stainless autoclave. The autoclave was heated to 200 °C and held for 12 h, after that the autoclave was cooled down to room temperature naturally. The obtained biochar was washed using deionized water, and then dried at 80 °C. Second, the dry biochar was mixed with aqueous solutions of KOH at the ratio of KOH : C is 2:1 (mass ratios), the resulting slurry was dried at 80 °C to remove excess water. The dried KOH-carbon mixtures were heated from room temperature to 450 °C and held at this temperature for 30 min, and then continues to increase to 650 °C and kept for another 30 min, subsequently, the temperature was activated to 800 °C for 1 h and then cooled down to room temperature. The whole activation process was performed in a nitrogen atmosphere with a heating rate 5 °C min^{-1}. The obtained samples were rinsed with 1 M HCl solution to remove residual inorganic impurities, then dried at 80 °C in oven to obtain OPC or SPC samples.

2.2. Structure characterization

The morphology and microstructure of porous carbons were characterized using SEM (FEI Quanta 450) and TEM (JEOL 2100). The pore structures of the as-prepared porous carbon samples were evaluated using nitrogen adsorption and desorption isotherms carried on TriStar II 3020 surface area & pore size analyzer (Micromeritics) at 77 K. The specific surface area was calculated using the Brunauer-Emmett-Teller (BET) and *t*-plot methods, respectively. The pore size distribution was calculated using the Density functional theory (DFT). The chemical composition and the electronic state of the element of the prepared porous carbons was analyzed using X-ray photoelectron spectroscopy (XPS) on an Axis Ultra (Kratos) XPS spectrometer. A water droplet (5 μL) was dripped onto the OPC and SPC tablets to measure the wettability of OPC and SPC using an optical contact angle meter (DSA 20, Krüss, Germany). The OPC and SPC tablets were prepared using tableting machine under 15 MPa.

2.3. Electrochemical measurements

The electrochemical properties of the porous carbon electrodes were investigated using a three-electrode system in 6 M KOH solution on an electrochemical working station (CHI660C, China) at room temperature. A platinum foil electrode and Hg/HgO electrode served as counter electrode and reference electrode, respectively. The work electrodes were prepared by the following process: porous carbon (80 wt%), conductive carbon black (10 wt%) and PVDF binder (10 wt%) were mixed homogeneously in a NMP solvent to form a slurry. The obtained slurry was coated onto a nickel foam used as current collector by a brush, and then the electrodes was dried at 80 °C to evaporate the solvent. The mass loading of the OPC or SPC on each nickel foam was approximately 2–3 mg cm^{-2}. Cyclic voltammetry (CV), galvanostatic charge-discharge (GCD) and electrochemical impedance spectroscopy (EIS) tests were carried out to investigate the electrochemical behavior of the OPC and SPC electrodes. The CV and GCD measurements of the OPC and SPC electrodes were performed in the operating potential window between −1 and 0 V, and the electrochemical impedance spectroscopy test was performed in a frequency range of 10 kHz to 0.01 Hz with an alternate current amplitude of 5 mV at open circuit potential.

The gravimetric specific capacitances of these electrodes were calculated from the galvanostatic discharge curves according to the following Eq. (1):

$$C = \frac{I \times \Delta t}{m \times \Delta V} \tag{1}$$

Where C (F g^{-1}) represents the specific capacitance of the active material, I (A) refers to the applied discharge current, ΔV (V) corresponds to the potential window during the discharge process, m (g) represents the mass loading of OPC or SPC on each electrode.

Moreover, symmetrical supcapacitors (SSCs) were assembled by SPC electrodes and a polypropylene membrane as separator. The electrochemical performance of the SSCs was evaluated using the CV and GCD methods.

The specific capacitance of SSCs was calculated from the discharge curves according to the following equation:

$$C_s = \frac{2I \times \Delta t}{m \times \Delta V} \tag{2}$$

Where C_s (F g^{-1}) represents the specific capacitance of the SSCs, I (A) refers to the applied discharge current, ΔV (V) corresponds to the potential window during the discharge process, m (g) represents the total mass loading of active materials on two electrodes.

The energy density and power density of the SSCs were calculated according to the following equations:

$$\mathrm{E} = \frac{1}{2 \times 3.6} C_s \Delta \mathrm{V}^2 \tag{3}$$

$$\mathrm{P} = \frac{3600 \times E}{t} \tag{4}$$

where E is the energy density (W h kg^{-1}), P is the power density (W kg^{-1}), and t is the discharge time (second).

Please cite this article in press as: H. Quan, et al., Hierarchically porous carbon derived from biomass: Effect of mesopore and heteroatom-doping on electrochemical performance, Appl. Surf. Sci. (2018), https://doi.org/10.1016/j.apsusc.2018.01.202

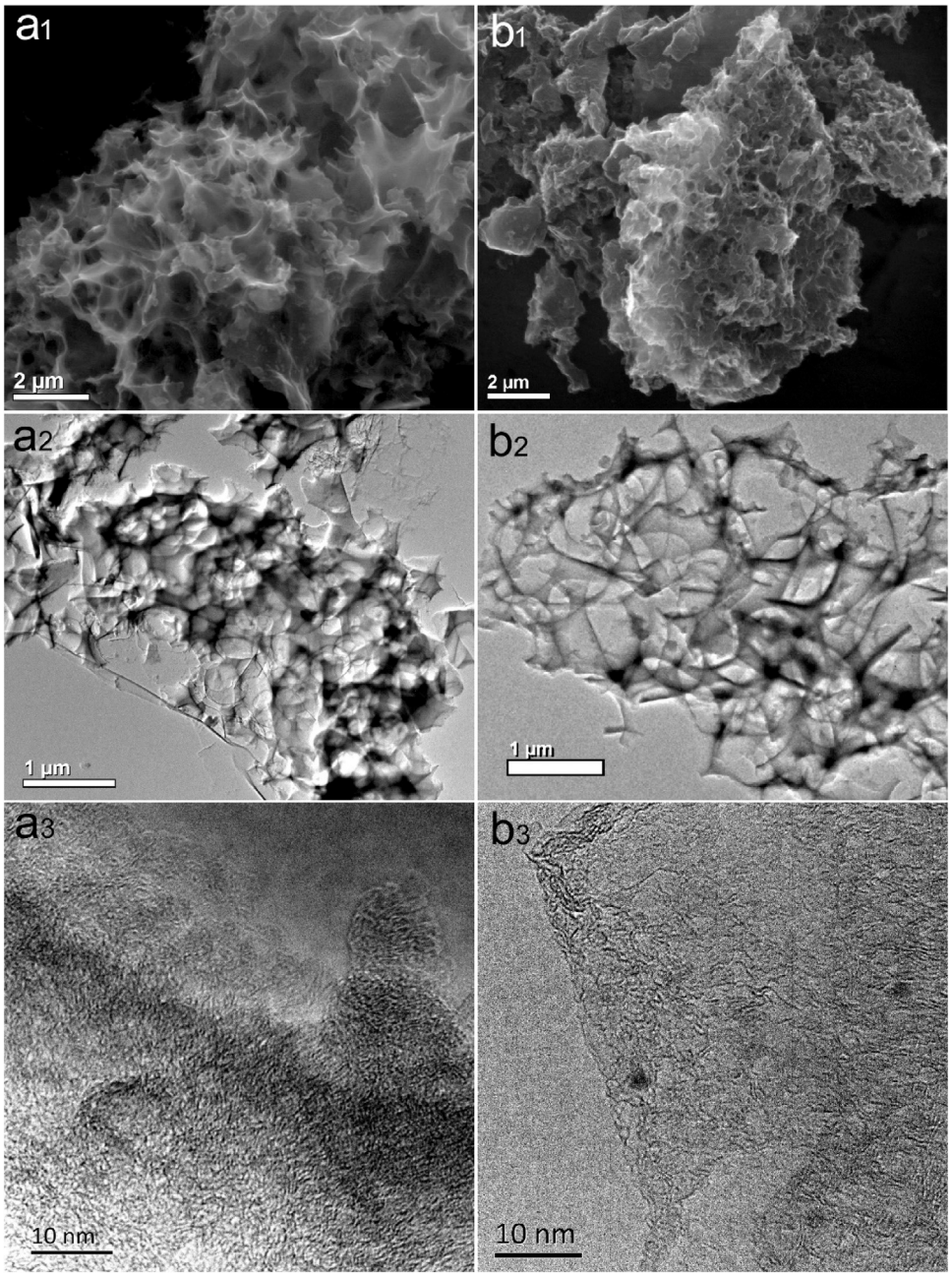

Fig. 1. Typical SEM and TEM images of (a_1–a_3) OPC and (b_1–b_3) SPC.

3. Results and discussion

3.1. Morphology and structure

Fig. 1 shows the typical SEM and TEM images of OPC and SPC samples. The OPC (Fig. 1a_1) possessed tremella-like structure while SPC shown honeycomb-like (Fig. 1b_1) structure. The detail of the morphological and structural of OPC and SPC were further observed using TEM. As displayed in Fig. 1a_2 and b_2, both carbon materials were consisted of many pores. These pores with sizes ranging from tens of nanometers to sub-micrometer were intertwined with each other to form a cross-linked carbon framework and difficultly to separate. In addition, the disorder structure shown in the typical HRTEM images (Fig. 1a_3 and b_3) indicated that the as-prepared OPC and SPC are amorphous, which are consistent with the reported porous carbons derived from other biomasses [15,31,32]. The XRD patterns of OPC and SPC are presented in Fig. S1 to further analyze the microstructure of these biomass-derived carbon materials. Two bread-like peaks at $2\theta = 26.2$ and 42.3 with low diffraction intensity indicates that both OPC and SPC samples have amorphous structure. In addition, the high intensity in the low-angle region suggests the presence of abundant micropores for theses carbon materials [14,15].

The pore structure, including the pore size and distribution, pore volume as well as special surface areas play a key role in the electrochemical behavior of ELDC. The pore structures of as-prepared OPC and SPC samples were analyzed by nitrogen adsorption/desorption method. The corresponding nitrogen adsorption/desorption isotherms of OPC and SPC samples were presented in Fig. 2a. Obviously, the OPC isotherm corresponds to an ideal type I isotherm according the IUPAC classification. The characteristic features of a sharp adsorption in low relative pressure

Please cite this article in press as: H. Quan, et al., Hierarchically porous carbon derived from biomass: Effect of mesopore and heteroatom-doping on electrochemical performance, Appl. Surf. Sci. (2018), https://doi.org/10.1016/j.apsusc.2018.01.202

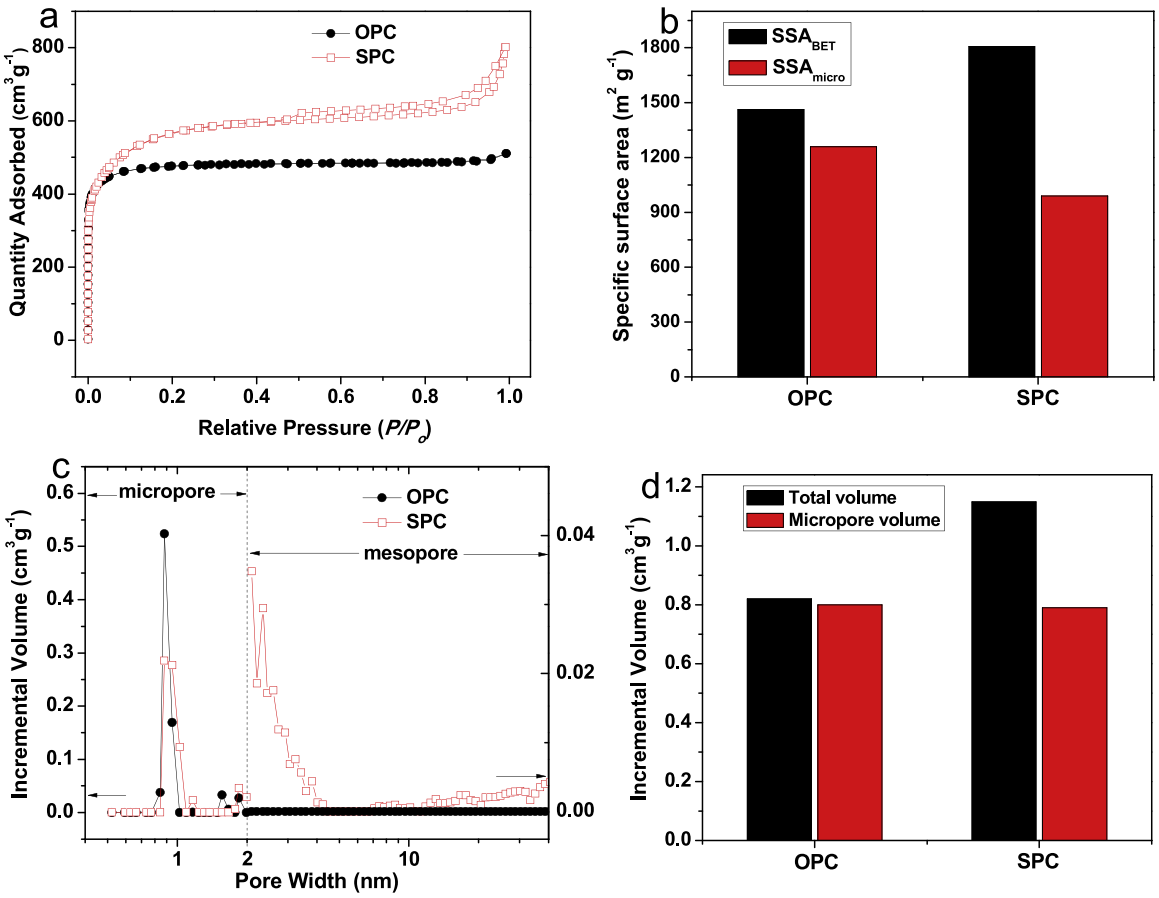

Fig. 2. a) Nitrogen adsorption/desorption isotherms of OPC and SPC; b) specific surface areas of OPC and SPC; c) pore-size distribution of OPC and SPC; d) pore volume of OPC and SPC.

($P/P_0 < 0.02$) and followed by a long horizontal plateau extending up to relatively high P/P_0 indicate that the pores in OPC are mainly microporous (pore widths <2 nm per IUPAC definition). Meanwhile, the N_2 adsorption isotherm of SPC is quite different with OPC, which exhibits a steep uptake below $P/P_0 < 0.02$ and a hysteresis loop above $P/P_0 > 0.5$, suggesting the co-presence of micropores and mesopores in the SPC samples. The specific surface area (SSA_{BET}) and micropore surface area (SSA_{micro}) of OPC and SPC samples were calculated from the corresponding N_2 adsorption isotherms using the BET and T-plot methods, respectively, and presented in Fig. 2b. The SSA_{BET} of OPC and SPC samples are 1462 and 1808 $m^2\ g^{-1}$, and the SSA_{micro} of OPC and SPC samples are 1259 and 990 $m^2\ g^{-1}$. Clearly, the SSA_{BET} of OPC is less than that of SPC, but the SSA_{micro} of OPC is much more than that of SPC. The pore size distribution curve of OPC calculated from the desorption data using the DFT method (Fig. 2c, black line) presents a unimodal-type pore size distribution with a peak at about 0.88 nm further confirms the microporous nature of OPC samples. On the contrary, the pore size distribution curve of SPC (Fig. 2c, red line) demonstrates the presence of both micropores and mesopore. Most of micropores fall into the size range of 0.88-1.02 nm, and the size of mesopores are mainly distributed in the ranges of 2–4 nm and 20–30 nm. As shown in Fig. 2d, the calculated total pore (size of pore less than 44 nm) volume of OPC and SPC is 0.82 and 1.15 $cm^3\ g^{-1}$, and the micropore volume of OPC and SPC is 0.8 and 0.79 $cm^3\ g^{-1}$, respectively. It indicates that the mesopore volume (0.36 $cm^3\ g^{-1}$) of SPC is obviously higher than that of OPC (0.02 $cm^3\ g^{-1}$). Compared to the OPC, the SPC possess not only many small size micropores (below 2 nm), but also a large amount of larger size mesopores (above 2 nm), which allows improved permeability of electrolytes [12,17,33,34]. In short, the SPC sample exhibits larger special surface areas, higher pore volume as well as optimal pore size distribution than OPC sample, which are crucial to improve the capacitance performance of EDLC [35].

3.2. Surface chemical analysis

It is well-known that the doping of electron-donating heteroatom such as O and N play a key role in the capacitance properties of the porous carbon materials for EDLC [1,18–21]. The chemical element and corresponding chemical state of OPC and SPC were analyzed using XPS, as shown in Fig. 3. The C and O are observed at 285 and 533 eV for both OPC and SPC, respectively. It is worth noting that one additional peak at 400 eV appears in the SPC, indicating that N element was also contained in the surface of the SPC samples. The atom percentage of carbon, oxygen, and nitrogen in OPC and SPC are listed in Table 1. The bonding configurations of N, C and O atoms were further identified by the high-resolution N 1s, C 1s and O 1s spectra, respectively. The N 1s spectra (Fig. 3b) of SPC could be fitted into four peaks at 398.5, 399.6, 400.7 and 402 eV, which are assigned to pyridinic-N (N-6), pyrrolic-N (N-5), quaternary-N (N-Q) and pyridinic N-oxide (N-X). The atomic percentages (Table 1) of these N species are 0.26, 0.49, 0.64 and 0.31%, respectively. The reported studies proposed that these N-containing groups of N-6 and N-5 can generate pseudocapacitance because of the possible reaction: [7,36].

$$-C=NH_2 + 2OH^- \leftrightarrow -C=NH + 2e^- + H_2O \quad (5)$$

$$-C-NH_2 + 2OH^- \leftrightarrow -C-NHOH + 2e^- + H_2O \quad (6)$$

Please cite this article in press as: H. Quan, et al., Hierarchically porous carbon derived from biomass: Effect of mesopore and heteroatom-doping on electrochemical performance, Appl. Surf. Sci. (2018), https://doi.org/10.1016/j.apsusc.2018.01.202

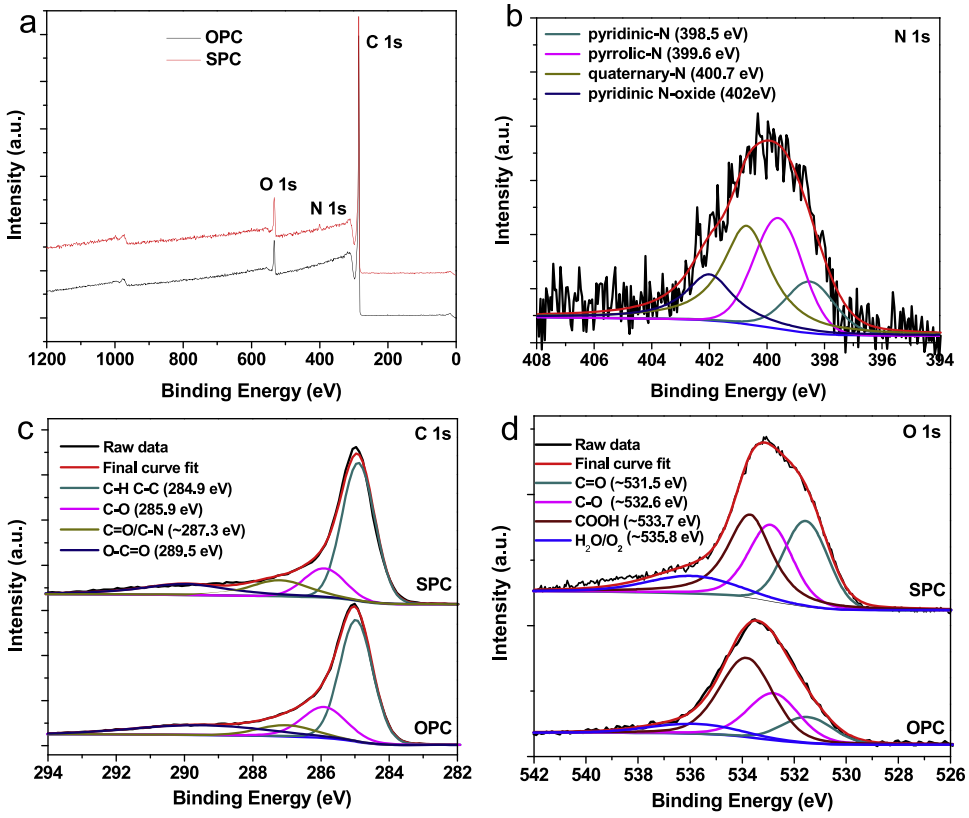

Fig. 3. XPS spectra of OPC and SPC samples; a) full spectrum, b) N1s spectra of SPC, c) C 1s spectra of OPC and SPC and d) O 1s spectra of OPC and SPC.

Table 1
Element composition (atomic%) in the surface of OPC and SPC.

Sample	Element content			Nitrogen content				Oxygen content			
	C	O	N	N-6	N-5	N-Q	N-X	C=O	C—O	COOH	H_2O/O_2
OPC	95.61	4.39						0.61	1.23	2.15	0.40
SPC	89.65	8.65	1.7	0.26	0.49	0.64	0.31	2.33	2.34	2.94	1.04

Additionally, N-Q can efficient improve the electron transfer of porous carbon materials [17]. The C 1s spectra (Fig. 3c) of OPC and SPC can be deconvoluted into four characteristic peaks, which can be attributed to carbon hydrocarbons (C—H and C—C at 284.9 eV, which are indistinguishable), hydroxyls or ethers (C=O) at 285.9 eV, carbonyls (C=O) at 287.3 eV or 287.2 eV, and carboxylic acids or esters (O—C=O) at 289.5 eV. The peak position of these chemical states have been well documented in the literature [37]. Interestingly, the peak at 287.3 eV for OPC shifts to 287.2 eV of SPC, and the intensity of the peak of SPC also increases, indicating the presence of C—N in the surface of SPC carbon materials. The O1s (Fig. 3d) spectra of OPC can be fitted to four characteristic peaks, corresponding to C=O (~531.5 eV), C—O (~532.6 eV), COOH (~533.7 eV), and adsorbed H_2O or O_2 (~535.7 eV), respectively. Compared to OPC, the peak positions of SPC shift slightly due to the chemical nature of the neighboring atoms on an individual surface. The quantitative analysis results in Table 1 indicate that the atomic ratio of oxygen in the SPC is 8.65%, which is more than that (4.39%) of the OPC. The more O-containing groups in the SPC can provide more pseudocapacitance due to the electrochemical reactions (Eq. (7)) at electrode interfaces [38].

$$-C=O+e^- \leftrightarrow -C-O^- \quad (7)$$

In addition, the percentage of C=O (2.33%) and C—O (2.34%) groups in the SPC is much more than those (only 0.61% and 1.23%, respectively) in OPC, but the percentage of COOH groups in SPC is near to those in OPC. According to the previous literature[39], the effect of surface functional groups on the capacitance was contingent on the type of functional groups in a way that the quinone-like C—O and the pyrone-like C=O functional groups were believed to increase the specific capacitance, while COOH behaved in the opposite way. The above XPS results suggest that the SPC will have higher specific capacitance than the OPC due to the presence of N-containing groups and the much more O-containing groups (C=O and C—O) in the surface of the SPC.

Additionally, previous literature[39] reported that the doping of heteroatom such as O and N to carbon materials can enhance the wettability of carbon materials. In the consequently, the wettability of OPC and SPC were characterized by a water droplet dripped onto the OPC and SPC tablets. The videos (Video S1 for OPC and Video S2 for SPC) show that a water droplet can spread out on the surface of OPC and SPC tablets completely during several seconds, suggesting that both OPC and SPC are hydrophilic. It demonstrates that the O or N containing groups on the surface of porous carbon materials can efficient improve the wettability of OPC and SPC. Besides, the spread speed of water droplet on SPC is slightly faster than that of OPC, which indicates that the wettability of SPC is higher than that

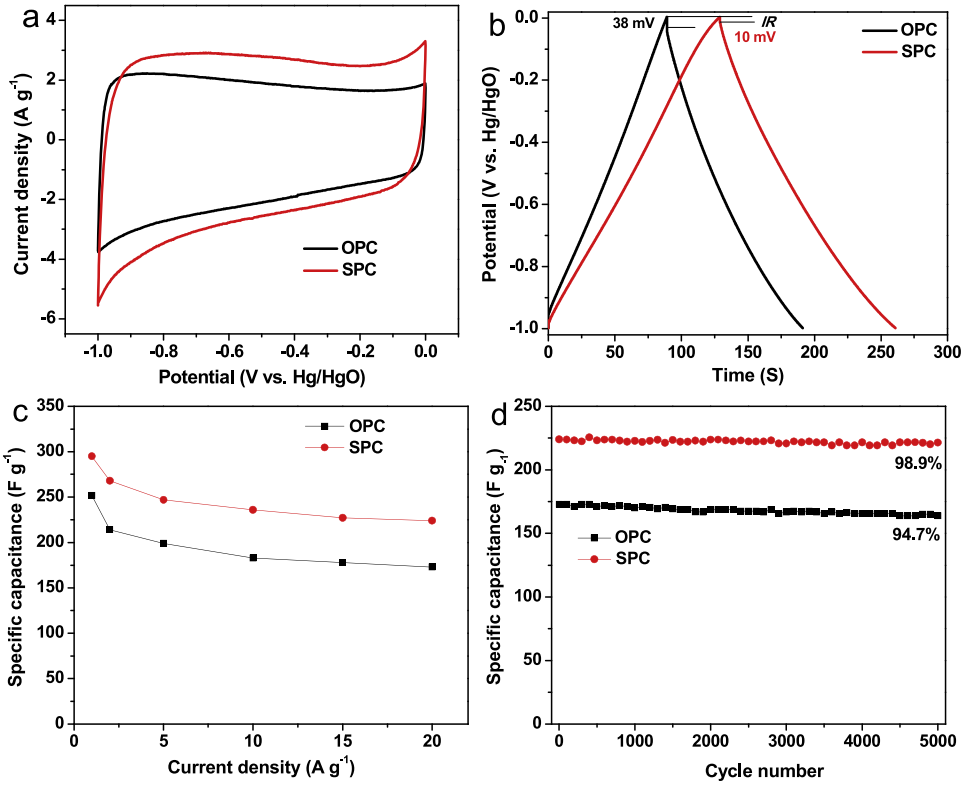

Fig. 4. a) CV curves of OPC and SPC electrodes at 10 mVs^{-1}; b) GCD curves of OPC and SPC electrodes under 2 A g^{-1}; c) specific capacitances of OPC and SPC electrodes at various current density; d) cycling stability of OPC and SPC electrodes measured at 10 A g^{-1}.

of OPC. It can be attributed to the high O content and the N-doping on the surface of SPC.

3.3. Electrochemical performance of OPC and SPC electrodes

The electrochemical performance of OPC and SPC electrodes was evaluated using CV and GCD methods in 6 M KOH aqueous at room temperature in a three-electrode system. Fig. 4a presents the CV curves of OPC and SPC electrodes, the distinct rectangular shape indicates the typical EDLC behavior of OPC and SPC. In addition, there is a small hump appears at around −0.9 V in the CV curves of OPC which correspond to the pseudocapacitive contribution of heteroatoms, namely O atoms in OPC [40]. The SPC electrode shows a similar CV curves with OPC but bigger areas based CV curves than OPC electrode, illustrates higher specific capacitance of SPC electrode. Notably, the small hump in SPC electrode shift slightly to around −0.8 V, suggesting that not only the O atoms but also N atoms contribute to the pseudocapacitive [15,17]. It is reported that heteroatoms, especially nitrogen atoms have electron-donor properties that can considerably improve the wettability of electrodes, enhance the conductivity as well as introduce additional pseudocapacitance [1,8,26,41,42].

Fig. 4b shows the GCD curves of OPC and SPC electrodes under a current density of 2 A g^{-1}. The triangular shape of GCD curves further confirm the idea EDLC behavior of OPC and SPC electrodes. In addition, the charge curves are almost symmetrical to their discharging counterparts. Besides, *IR* drop in charge/discharge curves was also investigated. Generally, *IR* drop is results from electrolyte potential drop and contact resistance, and depend on charge/discharge current density [43]. The *IR* drop for OPC and SPC electrodes is 38 and 10 mV at 2 A g^{-1}, respectively. According to the test process, larger *IR* drop of OPC electrode indicates that the contact resistance of OPC electrodes is higher than that the SPC electrodes. The specific capacitances of OPC and SPC electrodes were calculated from the discharge curve (Fig. S2) and shown in Fig. 4c. The specific capacitances of SPC electrodes are 295, 268, 247, 236, 227, and 224 F g^{-1} at 1, 2, 5, 10, 15, and 20 A g^{-1}, which is much higher than the corresponding capacitances of OPC electrodes (252, 214, 199, 183, 178, and 173 F g^{-1}). Furthermore, the capacitance retention (75.9%) of SPC is also superior than the OPC (68.6%) at 20 A g^{-1}. The cycling stability of SPC and OPC electrodes was analyzed by repeated charge-discharge process at the current density of 20 A g^{-1}. The specific capacitance of SPC is almost stable around 220 F g^{-1}, and still retained 98.9% of initial capacitance after 5000 cycles. Meanwhile, the OPC electrodes still delivered 164 F g^{-1} (94.7% of initial capacitance) after 5000 cycles. It indicates that the SPC electrodes exhibited better cycle stability than the OPC electrodes. To confirm the structural stability for SPC and OPC, Fig. 5 shows the TEM, the corresponding selected area electron diffraction (SAED) and HRTEM images of OPC and SPC after 5000 cycles. Although the tremella-like structure (Fig. 1a$_1$) of OPC and honeycomb-like structure (Fig. 1b$_1$) of SPC were destroyed during the TEM sample preparation, the macropores still can be observed in OPC (Fig. 5a) and SPC (Fig. 5c) after 5000 GCD cycles. In addition, no clear diffraction ring and diffraction spots in the corresponding SEAD (inset of Fig. 5a and 5c) and the disordered structure in the HRTEM images (Fig. 5b and d) of OPC and SPC indicate that both OPC and SPC are amorphous, which is consistent with the pristine OPC and SPC samples. Furthermore, some mesopores in SPC can be observed in Fig. 5d, which further confirms the effect of mesopores for the improvement of electrochemical performance of SPC.

The higher electrochemical performance of SPC electrodes than the corresponding OPC electrodes can be put down to the following aspects. Firstly, the abundant mesopores in SPC are beneficial for improved electrochemical performance. Although both OPC and

Please cite this article in press as: H. Quan, et al., Hierarchically porous carbon derived from biomass: Effect of mesopore and heteroatom-doping on electrochemical performance, Appl. Surf. Sci. (2018), https://doi.org/10.1016/j.apsusc.2018.01.202

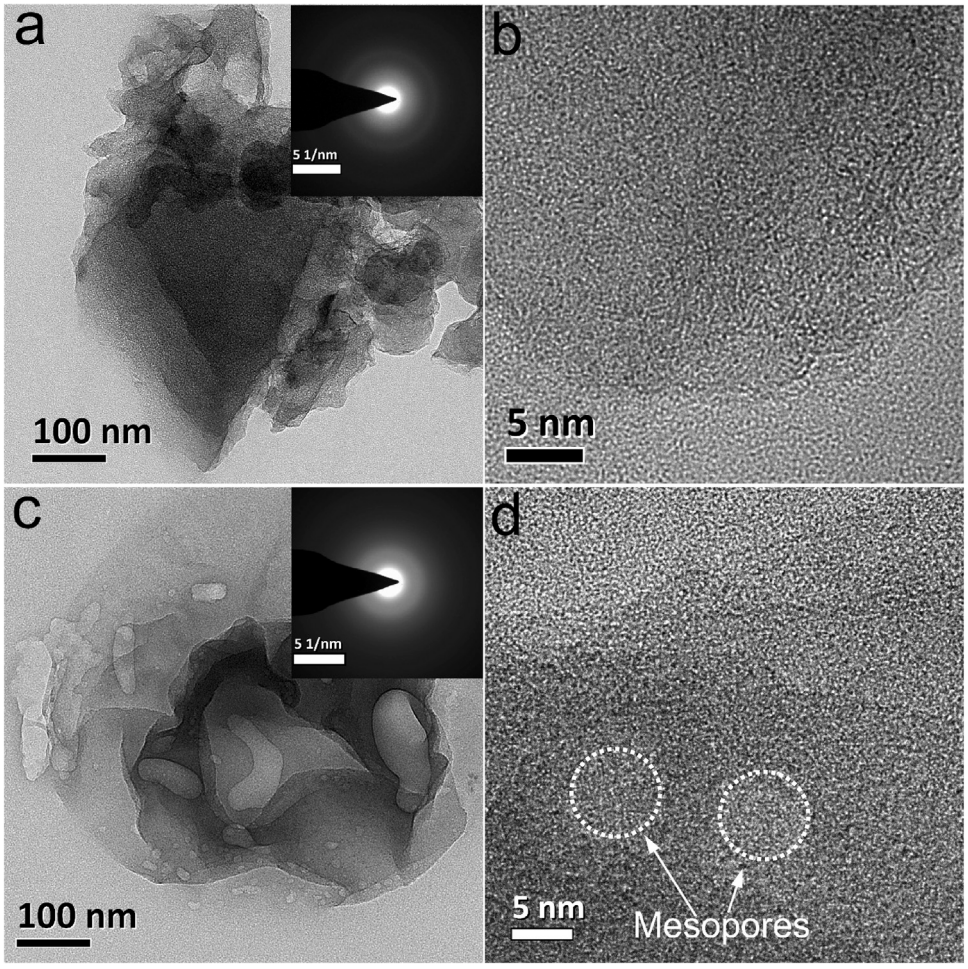

Fig. 5. TEM, corresponding SAED and HRTEM images of (a, b) OPC and (c, d) SPC after 5000 GCD cycles.

SPC have the structure of interpenetrating network, the mesopore volume (0.36 $cm^3 g^{-1}$) in SPC is significant higher than the OPC (0.02 $cm^3 g^{-1}$). The presence of abundant mesopore can not only effectively increase the contact between electrodes and electrolyte as well as accelerate mass transfer, but also bridge the micropores and the external environment [12,44,45], accordingly improve the electrochemical performance of SPC. Secondly, compared with the OPC, the nitrogen doping and more oxygen-containing groups in the surface of SPC also can improve the wettability of SPC and make an additional contribution to capacitance because they are electron-rich and can attract protons to the electrode surface. Finally, the abundant mesopores and the N-doping can effectively improve the electrical conductivity of SPC electrodes, which was further corroborated by electrochemical impedance spectroscopy (EIS) analysis. Fig. 6 shows the corresponding Nyquist plots and the results fitted with Zview software using equivalent circuit model in the inset. We can see that all the impedance spectra are composed of one semicircle in high frequency region and a linear part in low frequency region, illustration a typical behavior.[46] In high frequency region, the equivalent series resistance (R_s) of SPC electrodes (0.80 Ω) is lower than that of OPC electrodes (1.5 Ω). Besides, the diameter of semicircle at the high-frequency region represents the charge-transfer resistance (R_{ct}) at the electrode/electrolyte interface [47]. According to the semicircle diameter of fitted spectra, the Rct SPC electrodes is 0.26 Ω, which is slight smaller than that of the OPC electrodes (0.27 Ω). Furthermore, the low-frequency region of SPC plot is more vertical than the OPC, suggesting that the SPC electrodes have better capacitive behavior than OPC electrodes [48].

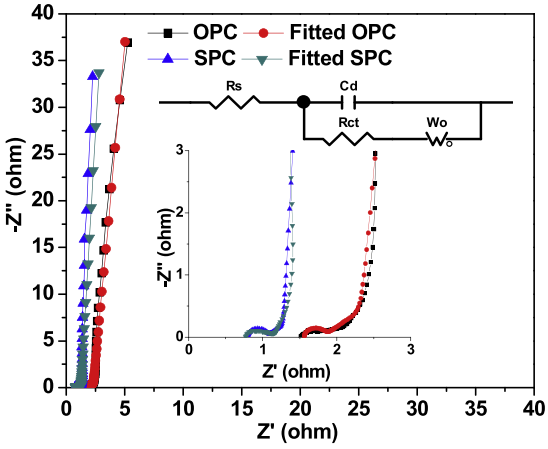

Fig. 6. Nyquist plots of OPC and SPC electrodes.

3.4. Electrochemical performance of SPC based symmetric supercapacitors

To further analyze the electrochemical performance of as-prepared SPC for supercapacitors, the symmetrical supercapacitors (SSCs) were fabricated by SPC electrodes. CV curves (Fig. 7a) of SSCs show the rectangular shapes in the voltage windows ranging from 0 to 1.0 V at different scan rates, even at 1000 mV s^{-1}, indicating the good EDLC behavior. It is further confirmed by the triangle shape of the GCD curves (Fig. 7b) at the current density of 1A g^{-1}. The specific

Please cite this article in press as: H. Quan, et al., Hierarchically porous carbon derived from biomass: Effect of mesopore and heteroatom-doping on electrochemical performance, Appl. Surf. Sci. (2018), https://doi.org/10.1016/j.apsusc.2018.01.202

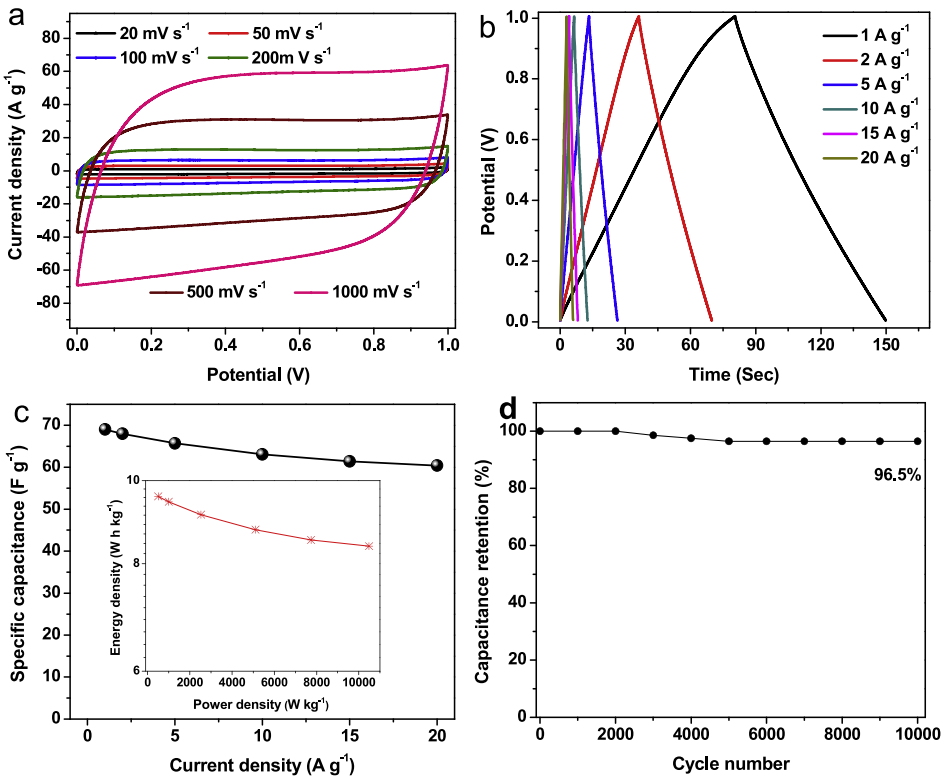

Fig. 7. Electrochemical performance of SSCs fabricated by SPC electrodes. a) CV curves at the scan rate of 50 mV s^{-1}; b) GCD curves at the current density of 1 A g^{-1}; c) specific capacitances at different current density (inset, Ragone plot of the power density against energy density); d) cycling stability at 20 A g^{-1}.

capacitances (Fig. 7c) of SSCs, calculated from the discharge curves shows that the SSCs deliver the specific capacitances of SSCs are 69 F g^{-1} at the current density of 1 A g^{-1}. When the current density increased to 20 A g^{-1}, the capacitances remain at 60.4 F g^{-1} with the retention of 87.5%, which indicates that the SSCs device has high rate capability. Furthermore, the Ragone plot of the energy density ***vs*** power density were presented in the inset of Fig. 7c. When the current density is 1 A g^{-1}, SPC fabricated SSCs can released an energy density up to 9.58 W h kg^{-1} at power density of 500 W kg^{-1}. With the current density increased to 20 A g^{-1}, the energy density of the SSCs remains 8.38 W h kg^{-1} at power density of 10 kW kg^{-1}. The stability of SSCs was tested using the GCD method at a current density of 20 A g^{-1}. Fig. 7d shows that the as-prepared SSCs device possesses excellent cycling stability and 96.5% capacitance retention is still retained after 10 000 cycles.

4. Conclusion

Osmanthus fragrans and *Sterculia lychnophora* were selected to prepare porous carbons of OPC and SPC using the two-step method including hydrothermal carbonization and KOH activation. The structure characterizations results revealed that OPC and SPC have the hierarchical micro/meso/macroporous structure with interpenetrating network, but the mesopore in SPC is obviously higher than OPC. The surface chemical analysis manifested that the SPC has nitrogen-containing groups and more oxygen-containing groups compared with OPC. Owing to the abundant mesopore, the doping of N and more oxygen-containing groups, the SPC electrodes delivered higher specific capacitance and higher capacitance retention than that of OPC used as electrode materials for EDLC. Finally, the SSCs device fabricated by SPC exhibited high energy density up to 9.58 W h kg^{-1} at power density of 500 W kg^{-1}. The electrochemical results showed that preparation of porous carbon materials from biomass is an effectively and low-cost procedure to improve high performance ELDC devices, and the selection of biomass precursors is the key for the preparation of high performance electrode materials for ELDC.

Acknowledgements

This work was supported by the National Natural Science Foundation of China (Grant No. 51402146; 51264033), the Aeronautical Science Foundation of China (Grant No. 2014ZF56021), the Natural Science Foundation of Jiangxi Province (Grant No. 20171BAB206046), and the Foundation of Nanchang Hangkong University (Grant No. EA201701386).

Appendix A. Supplementary data

Supplementary data associated with this article can be found, in the online version, at https://doi.org/10.1016/j.apsusc.2018.01.202.

References

[1] T. Lin, W. Chen, F. Liu, C. Yang, H. Bi, F. Xu, F. Huang, Nitrogen-doped mesoporous carbon of extraordinary capacitance for electrochemical energy storage, Science 350 (2015) 1508–1513.
[2] R.R. Salunkhe, Y.V. Kaneti, J. Kim, J.H. Kim, Y. Yamauchi, Nanoarchitectures for metal–organic framework-derived nanoporous carbons toward supercapacitor applications, Acc. Chem. Res. 49 (2016) 2796–2806.
[3] Y. Wang, Y. Song, Y. Xia, Electrochemical capacitors: mechanism, materials, systems, characterization and applications, Chem. Soc. Rev. 45 (2016) 5925–5950.
[4] W. Li, S. Liu, N. Pan, F. Zeng, Y. Liu, M. Zheng, Y. Liang, Post-treatment-free synthesis of highly mesoporous carbon for high-performance supercapacitor in aqueous electrolytes, J. Power Sources 357 (2017) 138–143.
[5] H. Pan, J. Yang, S. Wang, Z. Xiong, W. Cai, J. Liu, Facile fabrication of porous carbon nanofibers by electrospun PAN/dimethyl sulfone for capacitive deionization, J. Mater. Chem. A 3 (2015) 13827–13834.

[6] L.-F. Chen, X.-D. Zhang, H.-W. Liang, M. Kong, Q.-F. Guan, P. Chen, Z.-Y. Wu, S.-H. Yu, Synthesis of nitrogen-doped porous carbon nanofibers as an efficient electrode material for supercapacitors, ACS Nano 6 (2012) 7092–7102.
[7] T. Zhu, J. Zhou, Z. Li, S. Li, W. Si, S. Zhuo, Hierarchical porous and N-doped carbon nanotubes derived from polyaniline for electrode materials in supercapacitors, J. Mater. Chem. A 2 (2014) 12545.
[8] C. Su, C. Pei, B. Wu, J. Qian, Y. Tan, Highly doped carbon nanobelts with ultrahigh nitrogen content as high-performance supercapacitor materials, Small 13 (2017) 1700834.
[9] X. Wang, Y. Zhang, C. Zhi, X. Wang, D. Tang, Y. Xu, Q. Weng, X. Jiang, M. Mitome, D. Golberg, Y. Bando, Three-dimensional strutted graphene grown by substrate-free sugar blowing for high-power-density supercapacitors, Nat. Commun. 4 (2013) 2905.
[10] Y. Zhu, S. Murali, M.D. Stoller, K.J. Ganesh, W. Cai, P.J. Ferreira, A. Pirkle, R.M. Wallace, K.A. Cychosz, M. Thommes, D. Su, E.A. Stach, R.S. Ruoff, Carbon-Based supercapacitors produced by activation of graphene, Science 332 (2011) 1537–1541.
[11] J. Zhao, Y. Jiang, H. Fan, M. Liu, O. Zhuo, X. Wang, Q. Wu, L. Yang, Y. Ma, Z. Hu, Porous 3D few-layer graphene-like carbon for ultrahigh-power supercapa citors with well-defined structure-performance relationship, Adv. Mater. 29 (11) (2017) 1604569.
[12] J. Yang, H. Wu, M. Zhu, W. Ren, Y. Lin, H. Chen, F. Pan, Optimized mesopores enabling enhanced rate performance in novel ultrahigh surface area meso-/microporous carbon for supercapacitors, Nano Energy 33 (2017) 453–461.
[13] D. Zhu, Y. Wang, W. Lu, H. Zhang, Z. Song, D. Luo, L. Gan, M. Liu, D. Sun, A novel synthesis of hierarchical porous carbons from interpenetrating polymer networks for high performance supercapacitor electrodes, Carbon 111 (2017) 667–674.
[14] W. Wang, H. Quan, W. Gao, R. Zou, D. Chen, Y. Dong, L. Guo, N-Doped hierarchical porous carbon from waste boat-fruited sterculia seed for high performance supercapacitors, RSC Adv. 7 (2017) 16678–16687.
[15] Y. Dong, W. Wang, H. Quan, Z. Huang, D. Chen, L. Guo, Nitrogen-doped foam-like carbon plate consisting of carbon tubes as high-performance electrode materials for supercapacitors, ChemElectroChem 3 (2016) 814–821.
[16] C.Z. Yuan, B. Gao, L.F. Shen, S.D. Yang, L. Hao, X.J. Lu, F. Zhang, L.J. Zhang, X.G. Zhang, Hierarchically structured carbon-based composites: design, synthesis and their application in electrochemical capacitors, Nanoscale 3 (2011) 529–545.
[17] D. He, J. Niu, M. Dou, J. Ji, Y. Huang, F. Wang, Nitrogen and oxygen co-doped carbon networks with a mesopore-dominant hierarchical porosity for high energy and power density supercapacitors, Electrochim. Acta 238 (2017) 310–318.
[18] Y. Zhao, M. Liu, X. Deng, L. Miao, P.K. Tripathi, X. Ma, D. Zhu, Z. Xu, Z. Hao, L. Gan, Nitrogen-functionalized microporous carbon nanoparticles for high performance supercapacitor electrode, Electrochim. Acta 153 (2015) 448–455.
[19] H. Luo, Z. Liu, L. Chao, X. Wu, X. Lei, Z. Chang, X. Sun, Synthesis of hierarchical porous N-doped sandwich-type carbon composites as high-performance supercapacitor electrodes, J. Mater. Chem. A 3 (2015) 3667–3675.
[20] J. Zhou, J. Lian, L. Hou, J. Zhang, H. Gou, M. Xia, Y. Zhao, T.A. Strobel, L. Tao, F. Gao, Ultrahigh volumetric capacitance and cyclic stability of fluorine and nitrogen co-doped carbon microspheres, Nat. Commun. 6 (2015) 8503.
[21] L.-Z. Fan, S. Qiao, W. Song, M. Wu, X. He, X. Qu, Effects of the functional groups on the electrochemical properties of ordered porous carbon for supercapacitors, Electrochim. Acta 105 (2013) 299–304.
[22] C. Wang, D. Wu, H. Wang, Z. Gao, F. Xu, K. Jiang, Nitrogen-doped two-dimensional porous carbon sheets derived from clover biomass for high performance supercapacitors, J. Power Sources 363 (2017) 375–383.
[23] Z. Li, L. Zhang, B.S. Amirkhiz, X. Tan, Z. Xu, H. Wang, B.C. Olsen, C.M.B. Holt, D. Mitlin, Carbonized chicken eggshell membranes with 3D architectures as high-performance electrode materials for supercapacitors, Adv. Energy Mater. 2 (2012) 431–437.
[24] Z. Li, W. Lv, C. Zhang, B. Li, F. Kang, Q.-H. Yang, A sheet-like porous carbon for high-rate supercapacitors produced by the carbonization of an eggplant, Carbon 92 (2015) 11–14.
[25] S. Song, F. Ma, G. Wu, D. Ma, W. Geng, J. Wan, Facile self-templating large scale preparation of biomass-derived 3D hierarchical porous carbon for advanced supercapacitors, J. Mater. Chem. A 3 (2015) 18154–18162.
[26] J. Hou, C. Cao, F. Idrees, X. Ma, Hierarchical porous nitrogen-doped carbon nanosheets derived from silk for ultrahigh-capacity battery anodes and supercapacitors, ACS Nano 9 (2015) 2556–2564.
[27] H. Chen, D. Liu, Z. Shen, B. Bao, S. Zhao, L. Wu, Functional biomass carbons with hierarchical porous structure for supercapacitor electrode materials, Electrochim. Acta 180 (2015) 241–251.
[28] H. Sun, L. Cao, L. Lu, Bacteria promoted hierarchical carbon materials for high-performance supercapacitor, Energy Environ. Sci. 5 (2012) 6206–6213.
[29] Y. Lv, L. Gan, M. Liu, W. Xiong, Z. Xu, D. Zhu, D.S. Wright, A self-template synthesis of hierarchical porous carbon foams based on banana peel for supercapacitor electrodes, J. Power Sources 209 (2012) 152–157.
[30] Y. Gao, W. Zhang, Q. Yue, B. Gao, Y. Sun, J. Kong, P. Zhao, Simple synthesis of hierarchical porous carbon from Enteromorpha prolifera by a self-template method for supercapacitor electrodes, J. Power Sources 270 (2014) 403–410.
[31] W. Sun, S.M. Lipka, C. Swartz, D. Williams, F. Yang, Hemp-derived activated carbons for supercapacitors, Carbon 103 (2016) 181–192.
[32] J. Ma Y.-z. Dong L. Wang, P. Yu, H.-j. Yan, C.-g. Tian, J.-h. Li, H.-g. Fu, In–situ molten salt template strategy for hierarchical 3D porous carbon from palm shells as advanced electrochemical supercapacitors, ChemistrySelect 1 (2016) 2167–2173.
[33] H. Quan, B. Cheng, Y. Xiao, S. Lei, One-pot synthesis of α-Fe2O3 nanoplates-reduced graphene oxide composites for supercapacitor application, Chem. Eng. J. 286 (2016) 165–173.
[34] W. Gao, D. Chen, H. Quan, R. Zou, W. Wang, X. Luo, L. Guo, Fabrication of hierarchical porous metal–organic framework electrode for aqueous asymmetric supercapacitor, ACS Sustainable Chem. Eng. 5 (2017) 4144–4153.
[35] J. Yan, Q. Wang, T. Wei, Z. Fan, Recent advances in design and fabrication of electrochemical supercapacitors with high energy densities, Adv. Energy Mater. 4 (2014) 1300816.
[36] G.A. Ferrero, A.B. Fuertes, M. Sevilla, N-doped porous carbon capsules with tunable porosity for high-performance supercapacitors, J. Mater. Chem. A 3 (2015) 2914–2923.
[37] G.M. Burke, D.E. Wurster, M.J. Berg, P. Veng-Pedersen, D.D. Schottelius, Surface characterization of activated charcoal by X-ray photoelectron spectroscopy (XPS): correlation with phenobarbital adsorption data, Pharm. Res. 9 (1992) 126–130.
[38] H. Liu, H. Song, X. Chen, S. Zhang, J. Zhou, Z. Ma, Effects of nitrogen- and oxygen-containing functional groups of activated carbon nanotubes on the electrochemical performance in supercapacitors, J. Power Sources 285 (2015) 303–309.
[39] G. Milczarek, A. Ciszewski, I. Stepniak, Oxygen-doped activated carbon fiber cloth as electrode material for electrochemical capacitor, J. Power Sources 196 (2011) 7882–7885.
[40] C. Peng, J. Lang, S. Xu, X. Wang, Oxygen-enriched activated carbons from pomelo peel in high energy density supercapacitors, RSC Adv. 4 (2014) 54662–54667.
[41] W. Lu, M. Liu, L. Miao, D. Zhu, X. Wang, H. Duan, Z. Wang, L. Li, Z. Xu, L. Gan, L. Chen, Nitrogen-containing ultramicroporous carbon nanospheres for high performance supercapacitor electrodes, Electrochim. Acta 205 (2016) 132–141.
[42] S. Zhong, C. Zhan, D. Cao, Zeolitic imidazolate framework-derived nitrogen-doped porous carbons as high performance supercapacitor electrode materials, Carbon 85 (2015) 51–59.
[43] K. Wang, H. Wu, Y. Meng, Y. Zhang, Z. Wei, Integrated energy storage and electrochromic function in one flexible device: an energy storage smart window, Energy Environ. Sci. 5 (2012) 8384.
[44] A. Eftekhari, Z. Fan, Ordered mesoporous carbon and its applications for electrochemical energy storage and conversion, Mater. Chem. Front 1 (2017) 1001–1027.
[45] A.B. Fuertes, M. Sevilla, Hierarchical microporous/mesoporous carbon nanosheets for high-performance supercapacitors, ACS Appl. Mater. Interfaces 7 (2015) 4344–4353.
[46] H. Quan, B. Cheng, D. Chen, X. Su, Y. Xiao, S. Lei, One-pot synthesis of α-MnS/Nitrogen-doped reduced graphene oxide hybrid for high-performance asymmetric supercapacitors, Electrochim. Acta 210 (2016) 557–566.
[47] D. Chen, W. Wei, R. Wang, J. Zhu, L. Guo, α-Fe_2O_3 nanoparticles anchored on graphene with 3D quasi-laminated architecture: in situ wet chemistry synthesis and enhanced electrochemical performance for lithium ion batteries, New J. Chem. 36 (2012) 1589–1595.
[48] J. Kalupson, D. Ma, C.A. Randall, R. Rajagopalan, K. Adu, Ultrahigh-power flexible electrochemical capacitors using binder-free single-walled carbon nanotube electrodes and hydrogel membranes, J. Phys. Chem. C 118 (2014) 2943–2952.

Please cite this article in press as: H. Quan, et al., Hierarchically porous carbon derived from biomass: Effect of mesopore and heteroatom-doping on electrochemical performance, Appl. Surf. Sci. (2018), https://doi.org/10.1016/j.apsusc.2018.01.202